Inorganic Chemistry

Article

pubs.acs.org/IC

Syntheses, Structures, and Nonlinear Optical Properties of Quaternary Chalcogenides: $Pb_4Ga_4GeQ_{12}$ (Q = S, Se)

Yu-Kun Chen,[†,‡] Mei-Chun Chen, Liu-Jiang Zhou,[†,‡] Ling Chen,[†] and Li-Ming Wu*[,†]

[†]State Key Laboratory of Structural Chemistry, Fujian Institute of Research on the Structure of Matter, Chinese Academy of Sciences, Fuzhou, Fujian 350002, People's Republic of China

[‡]Graduate University of Chinese Academy of Sciences, Beijing 100039, People's Republic of China

Supporting Information

ABSTRACT: Two noncentrosymmetric isostructural compounds $Pb_4Ga_4GeQ_{12}$ (Q = S, Se) with their own structure type have been synthesized by solid-state reactions at high temperature. They crystallize in the tetragonal space group $P\bar{4}2_1c$ (No. 114) with a = 12.673(2) Å and c = 6.128(2) Å, and a = 13.064(7) Å and c = 6.310(5) Å, respectively, and Z = 2. The major structure motif features a three-dimensional framework constructed by chains of GaQ_4 tetrahedra that are interconnected by separated GeQ_4 tetrahedra at regular intervals. Interestingly, such a $[Ga_4GeQ_{12}]^{8-}$ framework is flexible to allow the addition of Ag^+ or Li^+ to occupy the embedded A- or B-type of vacancies to generate the previously reported $[AgGa_5Q_{12}]^{7-}$ or $[LiGa_5Q_{12}]^{7-}$ interstitial compounds without symmetry breaking. The title compounds (Q = S, Se) have optical band gaps of 2.35 and 1.91 eV, respectively, and wide IR transparent regions of 0.80−22.5 and 0.75−22.5 μm, respectively. Significantly, the powder $Pb_4Ga_4GeSe_{12}$ sample exhibits a strong second-harmonic-generation (SHG) response that is ∼2 times that of the benchmark $AgGaS_2$ at a laser radiation of 2.05 μm with a non phase-matchable behavior. The calculated d_{36} coefficient agrees well with the experimental observation. The density functional theory (DFT) calculations suggest that the SHG response originates from the electronic transitions from Se 4p states to Pb 6p, Ga 4p, and Ge 4p states.

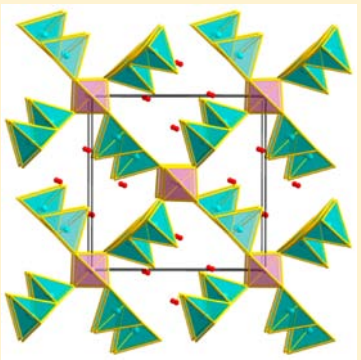

INTRODUCTION

Second-order nonlinear optical (NLO) materials produce new laser sources via the second-harmonic generation (SHG) and optical parametric oscillation processes; therefore, these materials are widely used in many fields, such as optical communication, laser surgery, molecular spectroscopy, and photochemistry.[1,2] The number of commercially available materials in mid-infrared (mid-IR) and far-IR regions are few—i.e., $AgGaS_2$,[3,4] $AgGaSe_2$,[5−7] and $ZnGeP_2$,[8]—but each of them unfortunately suffers drawbacks, such as low laser damage threshold or two-photon absorption. Therefore, the discovery of new effective IR NLO materials is of great importance and urgent need. The prerequisite of a NLO material is a crystallographic noncentrosymmetric (NCS) structure. In general, the parallel alignment of distorted tetrahedral building blocks are inclined to yield a NCS structure,[9] and numerous NCS chalcogenides have been thus discovered. Some of them—for example, $LiInS_2$,[10] $LiGaS_2$,[10] $BaGa_4S_7$,[11] and $BaGa_4Se_7$—exhibit outstanding NLO properties.[12] With regard to the Ge/Ga/Q (Q = S, Se, Te) system, a family of compounds with a general formula of $AGa_xGe_yQ_z$ is worthy of mention, e.g., $AgGaGeS_4$,[13] $Li_2Ga_2GeS_6$,[14] $LiGaGe_2Se_6$,[15] and $BaGa_2GeQ_6$ (Q = S, Se).[16] Among them, $BaGa_2GeSe_6$ is a phase-matchable material with a band gap of 2.81 eV and a large SHG coefficient (3.5 times that of benchmark $AgGaS_2$). These results stimulate our interest in such systems and we further consider that, except for the reported alkali metals, alkaline-earth metals, transition metals, and rare-earth metals,[13−17] main-group metal Pb^{2+} also may act as cation A in this system. The literature survey tells us that there are no quaternary Pb/Ga/Ge/Q chalcogenides yet: only a few Pb/Ge-containing chalcogenides are known, such as centrosymmetric (CS) Tl_2PbGeS_4,[18] $Na_8Pb_2(Ge_2S_6)_2$,[19] $Cs_4Pb_4Ge_5S_{16}$,[20] and $K_2PbGe_2S_6$,[20] and NCS Li_2PbGeS_4,[21] as well as $Na_{0.5}Pb_{1.75}GeS_4$ exhibiting a relative strong SHG response at a laser radiation of 3.5 μm (∼7−8 times that of $LiNbO_3$).[22] Meanwhile, only two CS Pb/Ga-containing chalcogenides are known: $Pb_2Ga_2S_5$[23] and $PbGa_2Se_4$.[24] In addition, Pb^{2+} is different than other metallic cation, because it has lone-pair electrons that may have some positive contribution to the polarization and overall SHG, as found in $Pb_2B_5O_9I$.[25] Therefore, we suppose that the combination of distorted GaQ_4 and GeQ_4 tetrahedra as anionic building units and Pb^{2+} as the cation may lead to some new NLO materials.

In this work, we successfully introduce the Pb^{2+} cation into Ga/Ge/Q system and discover two new NCS quaternary compounds: $Pb_4Ga_4GeQ_{12}$ (where Q = S, Se). The Se-member exhibits a SHG response that is ∼2 times larger than that of benchmark $AgGaS_2$ at a laser radiation of 2.05 μm, with a particle size of 30−46 μm. The SHG origin and the lone-pair character on the Pb^{2+} cation are discussed. An interesting

Received: November 15, 2012
Published: July 12, 2013

   dx.doi.org/10.1021/ic400995z | Inorg. Chem. 2013, 52, 8334−8341

structural relationship between the title compounds and $Ba_4AgGa_5Se_{12}$ and $Ba_4LiGa_5Se_{12}$[26] compounds is also reported.

EXPERIMENTAL SECTION

Synthesis. All acquired elements were stored inside an argon-filled glovebox with controlled moisture and oxygen levels, and all manipulations were carried out in the glovebox. Lead granule, gallium shot, and germanium, sulfur, and selenium powders (99.99% or higher) were purchased from Sinopharm Chemical Reagent Co., Ltd. The reagents were loaded in a silica tube and then flame-sealed under a high vacuum of 10^{-3} Pa. The reaction mixtures were heated in high-temperature tube furnaces, according to the profile described below.

$Pb_4Ga_4GeS_{12}$. The first synthesis attempt started from reactants with a 3:2:1:8 molar ratio of Pb:Ga:Ge:S. The mixture was heated at a rate of 24 °C/h to 980 °C and annealed at that temperature for 100 h, then subsequently cooled at a rate of ~6 °C/h to 350 °C, before switching off the furnace. The green crystal products were stable in air for a long time (more than six months). The single-crystal structure studies yielded a refined formula of $Pb_4Ga_4GeS_{12}$. After the establishment of the formula, a stoichiometric reaction of Pb:Ga:Ge:S in a silica crucible was carried out, which generated a pure phase of $Pb_4Ga_4GeS_{12}$, according to the powder X-ray diffraction (XRD) analysis (see Figure 1a). Semiquantitative energy-dispersive X-ray spectroscopy (EDX) analyses using a scanning electron microscopy (SEM) system on several clean and smooth green crystals revealed a stoichiometry of $Pb_{4.07(13)}Ga_{3.97(4)}Ge_{1.01(5)}S_{11.95(18)}$ (see Figure S1a in the Supporting Information) that agreed with the single-crystal refinement stoichiometry ($Pb_4Ga_4GeS_{12}$).

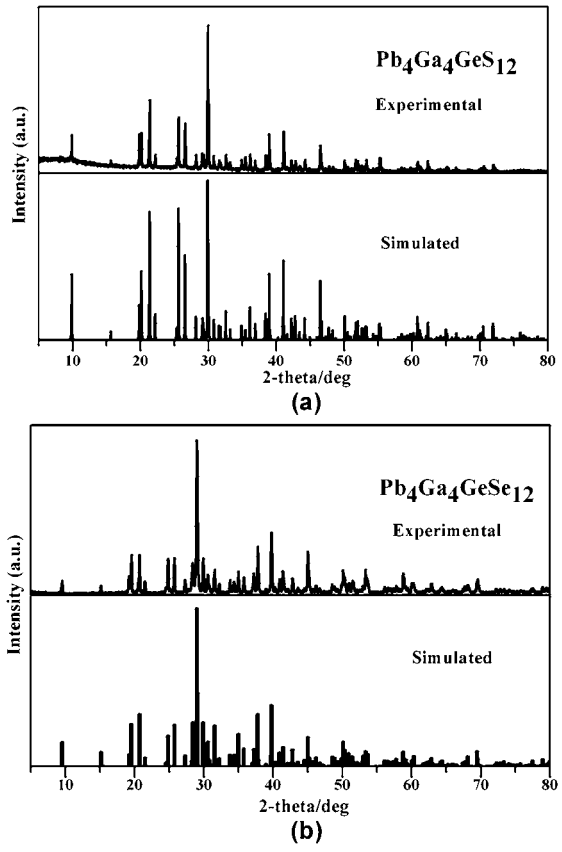

Figure 1. Experimental and simulated powder X-ray diffraction (XRD) patterns of (a) $Pb_4Ga_4GeS_{12}$ and (b) $Pb_4Ga_4GeSe_{12}$.

$Pb_4Ga_4GeSe_{12}$. Stoichiometric reactions were successful for the pure-phase selenide analogue, at 800 °C, which is a temperature that is 180 °C lower than that of the sulfide. The dark red crystals were refined as $Pb_4Ga_4GeSe_{12}$, using single-crystal diffraction data. These crystals were also stable in air for a long time (more than six months). The EDX result of $Pb_{3.85(19)}Ga_{3.82(25)}Ge_{1.00(1)}Se_{12.33(29)}$ was consistent with the single-crystal refinement results (see Figure S1b in the Supporting Information).

Single-Crystal X-ray Diffraction. Single-crystal XRD data were collected on a Rigaku Saturn724 CCD diffractometer with graphite-monochromated Mo Kα radiation (λ = 0.71073 Å) at 293 K. The data were corrected for Lorentz and polarization factors. Absorption corrections were performed by the multiscan method.[27] All structures were solved by the direct methods and refined by the full-matrix least-squares fitting on F^2 by SHELX-97.[28] Structures were verified by the ADDSYM algorithm via the PLATON program.[29] The assignments of Pb and three Q atoms were out of events, but it was difficult to assign Ga and Ge at the tetrahedral sites, M1 (8*e*) and M2 (2*a*), because of their similar X-ray scattering factors. Note that the molar ratio of Ga:Ge was close to 4:1, according to the EDX measurement. Second, the M2−Q bond was shorter than the M1−Q bond, i.e., M2−Se = 2.321(3) Å, M1−Se = 2.338(4)−2.394(4) Å; for comparison, in some of the structure-related compounds without disorder over the 8*e* and 2*a* sites, such as $Ba_4AgGa_5Se_{12}$ and $Ba_4LiGa_5Se_{12}$,[26] the Ga (2*a*)−Se distances (2.3997(8) or 2.4003(7) Å) were comparable with the Ga (8*e*)−Se distances (2.362(1)−2.427(1) or 2.380(1)−2.426(1) Å). Third, according to the valence bond sum (V_i),

$$V_i = \sum s_{ij}$$

where s_{ij} is the bond valence (defined as $s_{ij} = \exp[(R_{ij}-d_{ij})/0.37]$, where d_{ij} is the bond length between the nearest-neighboring atoms *i*−*j* and R_{ij} is the tabulated bond-valence parameter[30]). The M1 site was assigned as Ga (VBS = 2.98 for the S member, or 3.36 for the Se member) and M2 as Ge (VBS = 3.76 for the S member, or 4.32 for the Se member). Such an assignment generated a formula of $Pb_4Ga_4GeQ_{12}$, which satisfied the charge-balance requirement. Similar assignments were found in $Li_2Ga_2GeS_6$[14] and $Li_2Ga_2GeSe_6$.[15] Subsequently, according to such a stoichiometry, pure-phase $Pb_4Ga_4GeQ_{12}$ was successfully synthesized. Refinement results are shown in Table 1, the coordinates and thermal parameters are presented in Table 2, and selected bond lengths and angles are listed in Table 3. In addition, DFT optimizations of $Pb_4Ga_4GeSe_{12}$ have been carried out on models with different disorder patterns over M1 and M2 sites: model A (without disorder), and models B and C (with disorder). (See Table S1 in the Supporting Information.) According to the calculations, model A without disorder (i.e., 2Ge atoms occupy 2*a*

Table 1. Crystal Data and Structure Refinements for $Pb_4Ga_4GeS_{12}$ and $Pb_4Ga_4GeSe_{12}$

	$Pb_4Ga_4GeS_{12}$	$Pb_4Ga_4GeSe_{12}$
fw	1564.95	2127.75
crystal system	tetragonal	
crystal color	green	dark red
space group	$P\bar{4}2_1c$ (No. 114)	
a (Å)	12.673(2)	13.064(7)
b (Å)	12.673(2)	13.064(7)
c (Å)	6.128(2)	6.310(5)
V (Å^3)	984.1(3)	1076.8(1)
Z	2	
D_c (g cm^{-3})	5.281	6.562
μ (mm^{-1})	42.222	57.706
GOOF on F^2	1.089	1.058
R_1 ($I > 2\sigma(I)$)[a]	0.0585	0.0487
wR_2 ($I > 2\sigma(I)$)[b]	0.0927	0.1227
R_1 (all data)	0.0658	0.0554
wR_2 (all data)	0.0959	0.1263
absolute structure parameter	0.04(2)	−0.05(3)
largest diff. peak/hole (e Å^{-3})	2.02/−1.68	3.67/−3.17

[a] $R_1 = \sum||F_0| - |F_c||/\sum|F_0|$. [b] $wR_2 = [\sum w(F_0^2 - F_c^2)^2/\sum w(F_0^2)^2]^{1/2}$.

dx.doi.org/10.1021/ic400995z | Inorg. Chem. 2013, 52, 8334−8341

Table 2. Atomic Coordinates and Equivalent Isotropic Displacement Parameters of $Pb_4Ga_4GeQ_{12}$ (Q = S, Se)

atom	oxidation	Wyckoff	site occupation	x	y	z	U(eq)
			$Pb_4Ga_4GeS_{12}$				
Pb	+2	8e	1	0.6861(1)	0.9894(1)	0.5882(2)	0.032(1)
Ga (M1)	+3	8e	1	0.8518(2)	0.7645(2)	0.9509(4)	0.015(1)
Ge (M2)	+4	2a	1	1.0	1.0	1.0	0.017(1)
S1	−2	8e	1	0.9824(4)	0.6401(3)	0.9641(8)	0.017(1)
S2	−2	8e	1	0.9043(4)	0.9067(4)	0.7612(8)	0.016(1)
S3	−2	8e	1	0.7030(3)	0.6912(4)	0.8044(8)	0.018(1)
			$Pb_4Ga_4GeSe_{12}$				
Pb	+2	8e	1	0.6882(1)	0.9944(1)	0.5932(2)	0.033(1)
Ga (M1)	+3	8e	1	0.8507(2)	0.7658(2)	0.9479(4)	0.016(1)
Ge (M2)	+4	2a	1	1.0	1.0	1.0	0.016(1)
Se1	−2	8e	1	0.9845(2)	0.6407(2)	0.9597(4)	0.022(1)
Se2	−2	8e	1	0.9052(2)	0.9082(2)	0.7537(5)	0.034(1)
Se3	−2	8e	1	0.6983(2)	0.6918(2)	0.8060(4)	0.029(1)

Table 3. Selected Bond Lengths and Bond Angles for $Pb_4Ga_4GeQ_{12}$ (Q = S, Se)

	Bond Lengths (Å)	
	$Pb_4Ga_4GeS_{12}$	$Pb_4Ga_4GeSe_{12}$
Pb−Q1	2.827(5)	2.902(4)
Pb−Q1	2.882(5)	2.976(3)
Pb−Q1	3.075(4)	3.210(3)
Pb−Q2	3.142(6)	3.215(4)
Pb−Q3	2.991(5)	3.043(3)
Pb−Q3	3.375(5)	3.476(4)
Ge−Q2	2.239(5)	2.321(3)
Ge−Q2	2.239(5)	2.321(3)
Ge−Q2	2.239(5)	2.321(3)
Ge−Q2	2.239(5)	2.321(3)
Ga−Q2	2.245(5)	2.338(4)
Ga−Q3	2.271(6)	2.388(4)
Ga−Q3	2.286(5)	2.374(4)
Ga−Q1	2.287(6)	2.394(4)
	Bond Angles (deg)	
	$Pb_4Ga_4GeS_{12}$	$Pb_4Ga_4GeSe_{12}$
Q2−Ge−Q2	115.3(2)	116.63(9)
Q2−Ge−Q2	115.3(2)	116.63(9)
Q2−Ge−Q2	98.4(3)	95.9 (2)
Q2−Ge−Q2	98.4(3)	95.9(2)
Q2−Ge−Q2	115.3(2)	116.63(9)
Q2−Ge−Q2	115.3(2)	116.63(9)
Q2−Ga−Q3	114.8(2)	114.4(2)
Q2−Ga−Q3	111.5(2)	112.3(2)
Q3−Ga−Q3	104.5(2)	104.0(2)
Q2−Ga−Q1	111.0(2)	109.7(2)
Q3−Ga−Q1	105.3(2)	106.0(2)
Q3−Ga−Q1	109.3(2)	110.1(2)
Q2−Ge−Q2	98.4(3)	95.9 (2)
Q2−Ge−Q2	98.4(3)	95.9(2)
Q2−Ge−Q2	115.3(2)	116.63(9)
Q2−Ge−Q2	115.3(2)	116.63(9)
Q2−Ga−Q3	114.8(2)	114.4(2)
Q2−Ga−Q3	111.5(2)	112.3(2)
Q3−Ga−Q3	104.5(2)	104.0(2)
Q2−Ga−Q1	111.0(2)	109.7(2)
Q3−Ga−Q1	105.3(2)	106.0(2)
Q3−Ga−Q1	109.3(2)	110.1(2)

site, and 8Ga atoms occupy 8e site) is more stable than the other models with disorder. Such results support the single-crystal refinements well.

Powder X-ray Diffraction (XRD). The powder XRD patterns were collected on a PANalytical X'Pert Pro diffractometer at 40 kV and 40 mA, using Cu Kα radiation (λ = 1.5406 Å) at ambient temperature. Data were collected over a 2θ range of 5°−80°, with scan steps of 0.05°. The measured patterns were in good agreement with the simulated ones calculated from the single-crystal data (see Figure 1).

Elemental Analysis. Semiquantitative element analyses, according to energy-dispersive X-ray spectroscopy (EDX), were performed with the aid of a field-emission scanning electron microscope (FESEM) system (JEOL, Model JSM6700F) equipped with an energy-dispersive X-ray spectroscopy (EDX) system (Oxford INCA).

UV−Vis−Near-Infrared (NIR) and Infrared (IR) Spectroscopies. The optical diffuse reflectance spectra of polycrystalline samples were measured at room temperature, using a Perkin−Elmer Lambda 900 UV−Vis spectrophotometer equipped with an integrating sphere attachment and $BaSO_4$ as a reference in the range of 0.19−2.5 μm. The absorption spectrum was calculated from the reflection spectrum via the Kubelka−Munk function:

$$\frac{\alpha}{S} = \frac{(1-R)^2}{2R}$$

where α is the absorption coefficient, S the scattering coefficient, and R the reflectance.[31] The IR spectra were measured using a Perkin−Elmer Spectrum one FT-IR spectrophotometer in the range of 2.5−25 μm. Polycrystalline samples were ground with KBr and pressed into the form of transparent pellets for spectrum measurement.

Second-Harmonic-Generation (SHG) Measurements. The SHG response was measured on sieved polycrystalline samples on a modified Kurtz-NLO system, using 2.05 μm laser radiation.[32] The output signals were detected by a photomultiplier. The compound $Pb_4Ga_4GeSe_{12}$ was ground and sieved with particle sizes of 30−46, 46−74, 74−106, 106−150, and 150−210 μm, respectively. Powdered $AgGaS_2$ sieved in the same size range was used as a reference.

Computational Sections. The density functional theory (DFT) calculations were performed using the Vienna ab initio simulation package (VASP).[33] The generalized gradient approximation (GGA)[34] was chosen as the exchange-correlation functional and a plane wave basis with the projector augmented wave (PAW) potentials was used.[35] The plane-wave cutoff energy of 288 eV, and the threshold of 10^{-5} eV were set for the self-consistent-field convergence of the total electronic energy. Pseudo-atomic calculations were performed for Pb, $5d^{10}6s^26p^2$; Ge, $3d^{10}4s^24p^2$; Ga, $3d^{10}4s^24p^1$; S, $3s^23p^4$; and Se, $4s^24p^4$. The *k*-integration over the Brillouin zone was performed with the tetrahedron method,[36] using a 4 × 4 × 8 Monkhorst-Pack mesh. More than 300 empty bands were used in the calculations of optical properties. The scissors operator of 0.15 eV was applied for

dx.doi.org/10.1021/ic400995z | Inorg. Chem. 2013, 52, 8334−8341

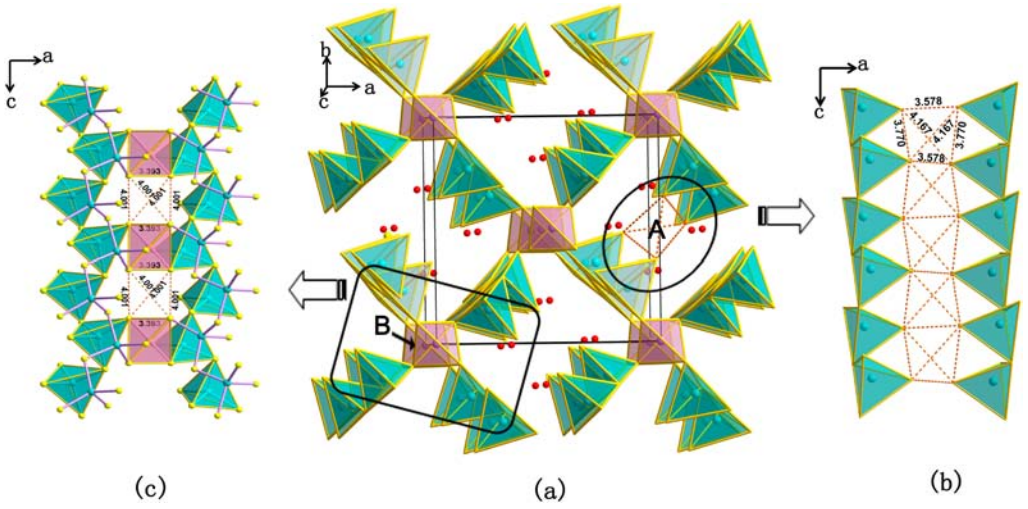

Figure 2. (a) View of the $Pb_4Ga_4GeQ_{12}$ structure with the unit cell marked and inter-A and inner-B vacancies indicated as dashed tetrahedra. (b) The inter-A vacancy between two GaQ_4 zigzag chains (the edge length is marked). (c) Side view of inner-B vacancy (the surrounding four parallel GaQ_4 chains are presented by polyhedron or ball-and-stick format). The Pb−Q bonds were omitted for the sake of clarity. Legend: red, Pb; light blue, Ga; pink, Ge; yellow, Q; light blue tetrahedron, GaQ_4; pink tetrahedron, GeS_4; dashed tetrahedron, inter-A or inner-B vacancy.

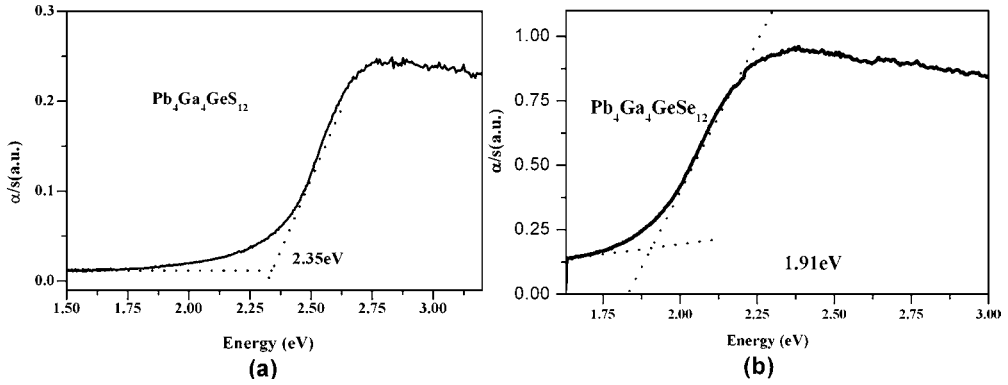

Figure 3. UV−Vis diffuse reflection spectra of (a) $Pb_4Ga_4GeS_{12}$ and (b) $Pb_4Ga_4GeSe_{12}$.

$Pb_4Ga_4GeSe_{12}$. The calculations of linear optical properties via the dielectric function $\varepsilon(\omega) = \varepsilon_1(\omega) + i\varepsilon_2(\omega)$ were carried out. The imaginary part $\varepsilon_2(\omega)$ was obtained from the Kubo−Greenwood formula.[37] The real part $(\varepsilon_1(\omega))$ was deduced from the Kramer−Kronig relationship.[38,39] The other optical constants could be derived from $\varepsilon_1(\omega)$ and $\varepsilon_2(\omega)$. The static and dynamic second-order nonlinear susceptibilities $\chi^{abc}(-2\omega, \omega, \omega)$ were calculated based on the so-called "length-gauge formalism", by Aversa and Sipe.[40,41]

RESULTS AND DISCUSSION

Crystal Structure. Compounds $Pb_4Ga_4GeQ_{12}$ (Q = S, Se) crystallize in the NCS tetragonal space group $P\bar{4}2_1c$ (No. 114) with a = 12.673(2) Å and 13.064(7) Å, respectively; c = 6.128(2) Å and 6.310(5) Å, respectively; and Z = 2. As shown in Figure 2a, the major structural motif is the three-dimensional (3D) network constructed by chains of GaQ_4 tetrahedra (light blue) (Figure 2) that are interconnected by separated GeQ_4 (pink) tetrahedra at regular intervals. Pb^{2+} cations locate between the chains. The chain of GaQ_4 tetrahedra is a zigzag chain along the c-direction formed by corner-sharing GaQ_4 tetrahedra (see Figure 2b), and four such parallel chains are grouped by separated GeQ_4 tetrahedra (pink) at regular intervals (see Figures 2a and 2c).

Uniquely, such a network accommodates two types of vacancies, as indicated by the dashed tetrahedron in Figure 2 (namely inter-A and inner-B). The inter-A vacancy is a tetrahedron centered by a 4d site, showing 2-fold rotation axis symmetry along the c-axis, which is lined up between two chains of GaQ_4 with Q−Q edges in the range of 3.578−4.167 Å (see Figure 2b). In comparison, the inner-B vacancy is a smaller tetrahedron centered by a 2b site, showing 4-fold screw axis symmetry along the c-direction, which is embedded between two separated GeQ_4 tetrahedra with Q−Q edges of 3.393−4.001 Å (see Figure 2c).

Interestingly, the larger inter-A vacancy can be occupied by a larger Ag^+ ion or the smaller inner-B vacancy can be occupied by a smaller Li^+ to generate two interstitial compounds, i.e., $Ba_4AgGa_5Se_{12}$ or $Ba_4LiGa_5Se_{12}$,[26] without changing the space group, the set of Wyckoff sites occupied, but with slightly enlarged unit-cell parameters. (See Figure S2 in the Supporting Information.) In the interstitial variants, Ba^{2+} corresponds to Pb^{2+}; Ga^{3+} occupies both 8e and 2a sites, which is occupied by Ga^{3+} or Ge^{4+} in the title compounds. As a result, the ionic network $[Ga_5Q_{12}]^{9-}$ in $Ba_4AgGa_5Se_{12}$[26] is one charge more negative than the $[Ga_4GeQ_{12}]^{8-}$ network in the title compound. Therefore, to keep the charge balance, Li^+ or Ag^+ cations are accommodated by the inner-B or the inter-A vacancy, as shown in Figure S2 in the Supporting Information. Such a structural relationship illustrates the flexibility of the network of the title compound, which also suggests that the

dx.doi.org/10.1021/ic400995z | Inorg. Chem. 2013, 52, 8334−8341

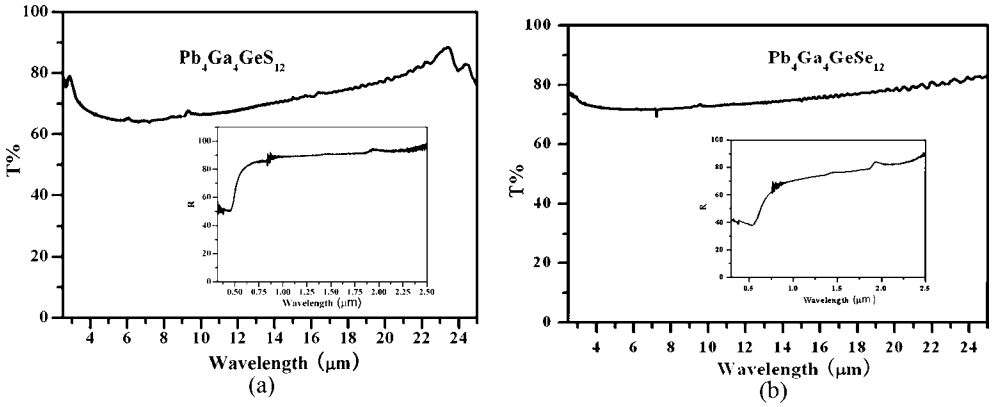

Figure 4. Reflection spectra (inset panel) and FT-IR spectra of (a) $Pb_4Ga_4GeS_{12}$ and (b) $Pb_4Ga_4GeSe_{12}$.

identities of such interstitial atoms can be controlled/selected by the oxide state of the $[M_4M']^{n-}$ framework. Therefore, it is reasonable to expect a series of new compounds with a general formula of $Pb_4A_xGa_{4+x}Ge_{1-x}Q_{12}$ ($0 \leq x \leq 1$). More interestingly, one can expect to adjust the band gap and the property, such as linear and nonlinear optical properties, by controlling the *x*-value and through the identity of the A-atom.

As listed in Table 2, there is one crystallographic distinguished Ga, Ge, and Pb atom, and there are three Q atoms in the structure. The Ga locating at the 8*e* site is 4-fold coordinated by Q in a distorted tetrahedron with Ga−S bonds of 2.245(5)−2.287(6) Å and S−Ga−S angles of 104.5°−114.8°; or Ga−Se of 2.338(4)−2.394(4) Å and Se−Ga−Se of 104.0°−114.4°. Whereas the Ge occupies 2*a* site centering a less-distorted tetrahedron with Ge−S = 2.239(5) Å and S−Ge−S = 98.4°−115.3°; or Ge−Se = 2.321(3) Å and Se−Ge−Se = 95.9°−116.63°. (See Table 3.) These values are similar to those observed in $Li_2Ga_2GeS_6$,[14] $Eu_2Ga_2GeS_8$,[17] and $LiGaGe_2Se_6$.[15] The Pb at the 8*e* site is coordinated with six Q atoms in a distorted octahedron (see Table 3, as well as Figure S3 in the Supporting Information) with a Pb−S bond length of 2.827(5)−3.375(4) Å or a Pb−Se bond length of 2.902(4)−3.476(3) Å. These distances are comparable to those observed in $Cs_4Pb_4Ge_5S_{16}$[20] and Li_2PbGeS_4.[21]

Optical Properties. $Pb_4Ga_4GeS_{12}$ and $Pb_4Ga_4GeSe_{12}$ are semiconductors with optical band gaps of ∼2.35 eV and ∼1.91 eV (see Figure 3). These are consistent with their colors (green or red) and smaller than those of $Ba_4AgGa_5Se_{12}$ (2.52 eV), $Ba_4LiGa_5Se_{12}$ (2.65 eV), as well as $AgGaS_2$ (2.56 eV),[17] $ZnGeP_2$ (2.0 eV), and $AgGaSe_2$ (1.8 eV). Their IR transparent ranges are 0.80−22.5 μm for $Pb_4Ga_4GeS_{12}$ and 0.75−22.5 μm for $Pb_4Ga_4GeSe_{12}$, as indicated by the IR and diffuse reflectance spectra (see Figure 4). These are comparable to those reported for $AgGaS_2$ (0.60−23 μm)[17] and $Eu_2Ga_2GeS_7$ (0.65−21 μm).[17] The title compounds are noncentrosymmetric (NCS), polar, and transparent in the mid-IR region; thus, their SHG properties at room temperature have been investigated on polycrystalline samples. The particle size versus SHG intersity of $Pb_4Ga_4GeSe_{12}$ indicates a non phase-matchable behavior at a laser radiation of 2.05 μm. (See Figure S4 in the Supporting Information.) As shown in Figure 5, $Pb_4Ga_4GeSe_{12}$ is ∼2 times more efficient than the commercial $AgGaS_2$ at a particle size of 30−46 μm. However, the SHG effect on $Pb_4Ga_4GeS_{12}$ at a laser radiation of 2.05 μm is not observed. In addition, the NLO properties of structure-related compounds $Ba_4AgGa_5Se_{12}$ and $Ba_4LiGa_5Se_{12}$ had not been reported yet.[26]

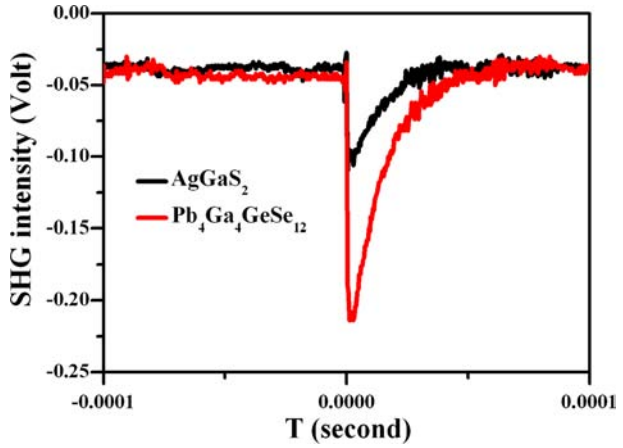

Figure 5. Plot of the relative SHG signals of $Pb_4Ga_4GeSe_{12}$ and $AgGaS_2$ (particle sizes of 30−46 μm were used for the SHG efficiency comparison).

Theoretical Studies. The band structures are plotted in Figure 6. The tops of the valence bands (VB) are located at point M, and the bottoms of the conduction bands are located at point A, indicating indirect band gaps of 2.16 and 1.76 eV for $Pb_4Ga_4GeS_{12}$ and $Pb_4Ga_4GeSe_{12}$, respectively. The calculated band gaps are consistent with the experimental values (2.35, 1.91 eV) derived from the UV−vis diffuse reflection spectra.

The total and partial densities of states (DOS and PDOS, respectively) for $Pb_4Ga_4GeSe_{12}$ are shown in Figure 7. The top of the valence band (VB) contains significant contributions from Se 4p states, and the bottom of the conduction band (CB) originates from Pb 6p, Se 4p, and small amounts of Ga 4s and Ge 4s states. The optical absorptions for $Pb_4Ga_4GeSe_{12}$ is mainly ascribed to the charge transition from Se 4p to Pb 6p states. In the VB-3 region (from −15 eV to −11 eV), the major contribution is Se 4s (88%). The VB-2 region, from −11 eV to −4 eV, is primarily derived from Pb 6s (37.6%), Se 4p (21.3%), Ga 4s (21.8%), and Ge 4s (5.0%). The VB-1 region (from −4 eV to the Fermi energy (E_F)) primarily derives from Se 4p (76.4%) hybridized with Ga 4p (8.9%) and Ge 4p (2.8%), indicating strong Ga−Se and Ge−Se covalent interactions. In addition, the contributions of Pb 6s (3.0%) and Pb 6p (6.0%) to VB-1 and VB-2 are smaller, which means 6s electrons on Pb^{2+} weakly interact with Se 4p in these regions. Above E_F, the components of each region are described as follows: CB-1: Se 4p (30.6%), Pb 6p (35.0%), Ga 4s (12.5%), and Ge 4s (5.8%); CB-2: Se 4p (39.2%), Pb 6p (22.8%), Ga 4p (20.3%), and Ge

dx.doi.org/10.1021/ic400995z | Inorg. Chem. 2013, 52, 8334−8341

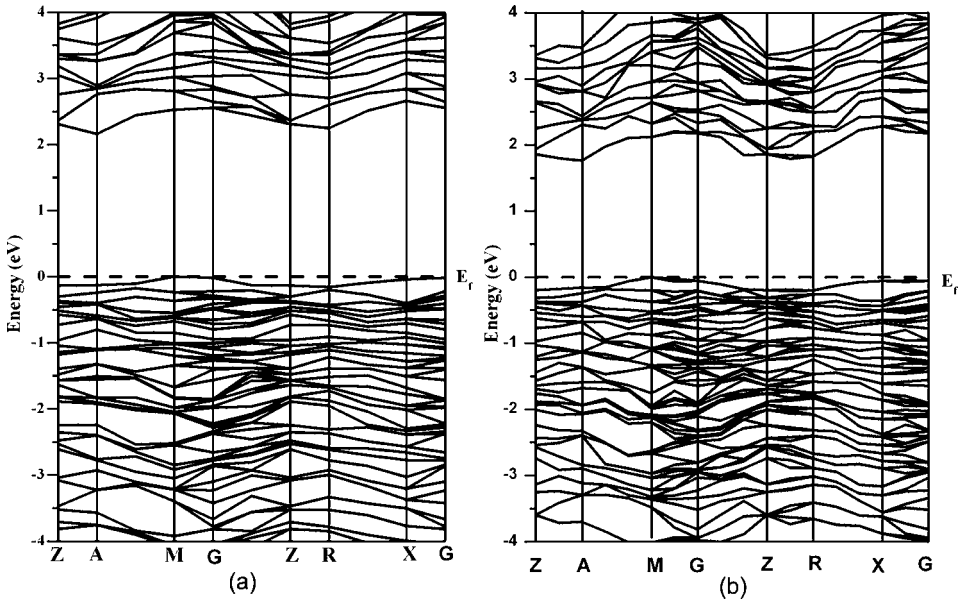

Figure 6. Calculated band structures of (a) $Pb_4Ga_4GeS_{12}$ and (b) $Pb_4Ga_4GeSe_{12}$.

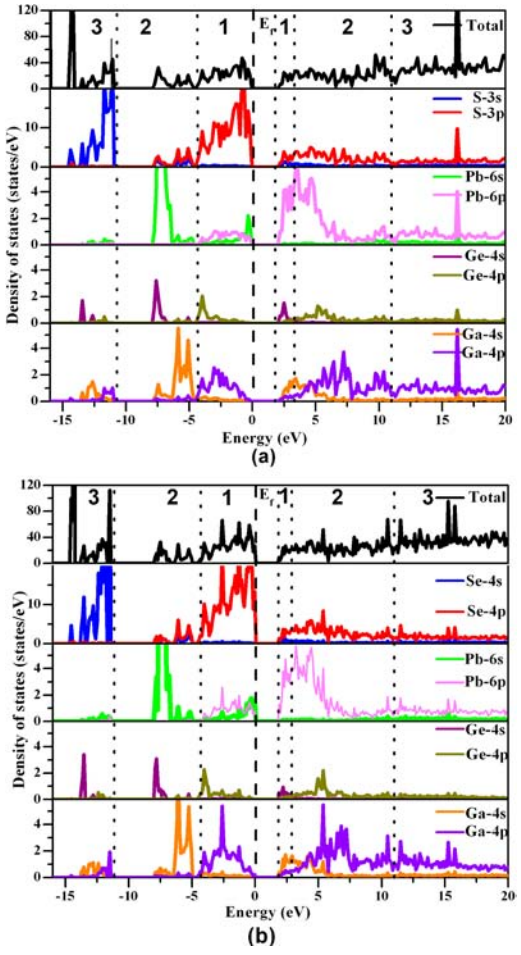

Figure 7. Total and partial density of states (DOS and PDOS, respectively) for (a) $Pb_4Ga_4GeS_{12}$ and (b) $Pb_4Ga_4GeSe_{12}$. Dashed line represents the Fermi energy (E_f), whereas the dotted lines denote different regions in the valence band (VB) and conduction band (CB).

4p (5.6%); CB-3: Se 4p (39.3%), Ga 4p (22.2%), and Pb 6p (17.4%).

Electron localization function (ELF) calculations were performed to examine the lone-pair stereochemical activity on the Pb^{2+} cation. The ELF with $\eta = 0.7$ indicates a spherelike isosurface at the Pb^{2+} site, which means the 6s electrons are stereochemically inert.[25,42] (See Figure S5 in the Supporting Information.) This may be ascribed to the relatively symmetric PbQ_6 coordination geometry. In the case of a more-distorted PbO_7I_2 polyhedron made by anions with significantly different electronegativities in $Pb_2B_5O_9I$, Pb^{2+} is stereochemical active.[25] However, in title compound $Pb_4Ga_4GeSe_{12}$, such an electronegativity-difference induction does not exist; therefore, the stereochemical activity of Pb^{2+} centered on the $PbSe_6$ octahedron is not remarkable, despite the geometry distortion. Consequently, the polarization associated with the Pb^{2+} cation should be negligible in the title $Pb_4Ga_4GeQ_{12}$ compounds.

The optical properties of $Pb_4Ga_4GeSe_{12}$ have been calculated. The macroscopic linear optical response of material is represented by the dielectric function $\varepsilon(\omega) = \varepsilon_1(\omega) + i\varepsilon_2(\omega)$. The imaginary part $(\varepsilon_2(\omega))$ originates from the contribution of the interband transition, while the intraband transition is ignored, because it is only significant in metallic compounds.[43] The energy dependence of the real part $(\varepsilon_1(\omega))$ and the imaginary part $(\varepsilon_2(\omega))$ is displayed in Figure S6 in the Supporting Information. The average value of the polarized zero-frequency dielectric constant is 9.78, which is calculated from the equation

$$\varepsilon_1(0) = \frac{1}{3}\left[\varepsilon_{1xx}(0) + \varepsilon_{1yy}(0) + \varepsilon_{1zz}(0)\right]$$

The main peak of the imaginary part, $\varepsilon_2(\omega)$, is located at ~3.7 eV, which is mainly regarded as the electronic interband transition from the Se 4p state to the Pb 6p state. The refractive index $(n(\omega))$, absorption coefficient $(I(\omega))$, and reflectivity $(R(\omega))$ are also calculated. (See Figure S7 in the Supporting Information.) The function $n(\omega)$ exhibits its peak value at ~2.7 eV and rapidly decreases in the region from 3.0 eV to 13.0 eV, corresponding mainly to the higher values for $R(\omega)$ in this range. Because of the free carrier adsorptions in semiconductors,[37] the absorption coefficient $I(\omega)$ is very large ($\sim 10^5$ cm^{-1}), and the calculated absorption edge is 2.0 eV. The

dx.doi.org/10.1021/ic400995z | Inorg. Chem. 2013, 52, 8334−8341

static birefringence (Δn) is found to be 0.0504, which is compared with that of $AgGaS_2$ (0.039).[17] The highest Δn value (0.625) occurs at ~2.67 eV.

The title compounds belong to the point group $\bar{4}2m$, showing two nonvanishing second-order susceptibility tensors (χ_{14}, χ_{36}). Under the restriction of Kleinman's symmetry, only one independent SHG tensor (χ_{36}) remains. In addition, the static calculated SHG coefficient (d_{36}) of $Pb_4Ga_4GeSe_{12}$ is 40 pm/V. The dynamic coefficients d_{36} of $Pb_4Ga_4GeSe_{12}$ and $AgGaS_2$ (as reference) are shown in Figure S8 in the Supporting Information. The calculated d_{36} coefficient is 54.5 pm/V at λ = 2.05 μm (0.61 eV), which is much higher than that of $AgGaS_2$ (18.21 pm/V). The cutoff-energy dependence of the static SHG coefficient d_{36} is also studied to explore the origin of the SHG response. As shown in Figure 8, the origin of the SHG

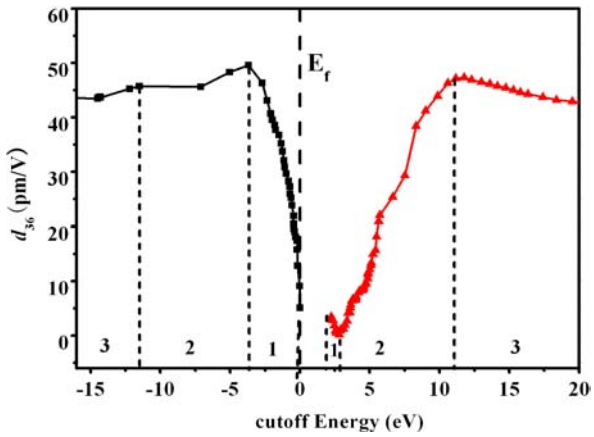

Figure 8. Cutoff-energy-dependent static SHG coefficients of $Pb_4Ga_4GeSe_{12}$. Dashed line represents E_f; dotted lines denote different regions in the VB and CB.

response is dominated by the VB-1 and CB-2 regions. The VB-1 region is mainly Se 4p states and CB-2 has contributions mostly from Se 4p, Pb 6p, Ga 4p, and Ge 4p states. The lone pairs on Pb^{2+} are not stereochemically activated and have no contribution to the polarization. Consequently, the SHG response is mainly ascribed to the electronic transitions from the Se 4p state to the Pb 6p, Ga 4p, and Ge 4p states.

CONCLUSION

In summary, two noncentrosymmetric compounds—$Pb_4Ga_4GeQ_{12}$ (Q = S, Se), with their own structure type—were discovered via solid-state reactions. The featured $[Ga_4GeQ_{12}]^{8-}$ anionic three-dimensional (3D) network is constructed by chains of GaQ_4 tetrahedra that are interconnected by separated GeQ_4 at regular intervals; Pb^{2+} cations are located between the chains. Interestingly, two types of irregular tetrahedron vacancies embedded in such a framework can be occupied by Ag^+ or Li^+ cations to generate two previously reported $[AgGa_5Q_{12}]^{7-}$ and $[LiGa_5Q_{12}]^{7-}$ intestinal compounds[26] without changing the symmetry. Such a structure flexibility, in association with different interstitial atoms and substitution of Ge atoms by Ga atoms, predicts a series of compounds with a general formula of $Pb_4A_xGa_{4+x}Ge_{1-x}Q_{12}$, with which the modulations of the band gap and the NLO property is highly possible via adjustment of the x-value and the identity of the A-atom.

The optical band gaps of the title compounds are measured to be 2.35 and 1.91 eV, which are consistent with their colors and the calculated results. Both compounds have wide infrared (IR)-transparent regions. Remarkably, the polycrystalline $Pb_4Ga_4GeSe_{12}$ sample exhibits a strong second-harmonic-generation (SHG) response, ~2 times greater than the benchmark $AgGaS_2$ at a laser radiation of 2.05 μm, with a non phase-matchable behavior. The calculated d_{36} coefficient agrees with the experimental observations. Especially, the lone pairs on Pb^{2+} hardly contribute to the polarization. The SHG response mainly originates from the charge transitions from Se 4p states to Pb 6p, Ga 4s, and Ge 4s states. Further exploration on the predicted $Pb_4A_xGa_{4+x}Ge_{1-x}Q_{12}$ compounds is worthwhile.

ASSOCIATED CONTENT

Supporting Information

CIF data, experimental methods, and additional tables and figures. This material is available free of charge via the Internet at http://pubs.acs.org.

AUTHOR INFORMATION

Corresponding Author

*Tel.: (011)86-591-83705401. E-mail: liming_wu@fjirsm.ac.cn.

Notes

The authors declare no competing financial interest.

ACKNOWLEDGMENTS

This research was supported by the National Natural Science Foundation of China (under Project Nos. 21225104, 20973175, 21171168, 21233009, and 90922021) and the "Knowledge Innovation Program of the Chinese Academy of Sciences" (Grant No. KJCX2-YW-H20).

REFERENCES

(1) (a) Chen, C. T.; Liu, G. Z. *Annu. Rev. Mater. Sci.* **1986**, *16*, 203. (b) Burland, D. M. *Chem. Rev.* **1994**, *94*, 1. (c) Bordui, P. F.; Fejer, M. M. *Annu. Rev. Mater. Sci.* **1993**, *23*, 321. (d) Chen, W.; Mouret, G.; Boucher, D.; Tittel, F. K. *Appl. Phys. B: Laser Opt.* **2001**, *72*, 873.

(2) (a) Liao, J. H.; Marking, G. M.; Hsu, K. F.; Matsushita, Y.; Ewbank, M. D.; Borwick, R.; Cunningham, P.; Rosker, M. J.; Kanatzidis, M. G. *J. Am. Chem. Soc.* **2003**, *125*, 9484. (b) Bera, T. K.; Jang, J. I.; Ketterson, J. B.; Kanatzidis, M. G. *J. Am. Chem. Soc.* **2009**, *131*, 75. (c) Zhang, Q.; Chung, I.; Jang, J. I.; Ketterson, J. B.; Kanatzidis, M. G. *J. Am. Chem. Soc.* **2009**, *131*, 9896. (d) Banerjee, S.; Malliakas, C. D.; Jang, J. I.; Ketterson, J. B.; Kanatzidis, M. G. *J. Am. Chem. Soc.* **2008**, *130*, 12270.

(3) Boyd, G. D.; Kasper, H.; Mcfee, J. H. *IEEE J. Quantum Electron.* **1971**, QE 7, *12*, 563.

(4) Harasaki, A.; Kato, K. *Jpn. J. Appl. Phys.* **1997**, *36*, 700.

(5) Tell, B.; Kasper, H. M. *Phys. Rev. B* **1971**, *4*, 4455.

(6) Kasper, H. M. *J. Electrochem. Soc.* **1972**, *119*, C96.

(7) Airoldi, G.; Beucherie, P.; Rinaldi, C. *J. Cryst. Growth.* **1977**, *38*, 239.

(8) Boyd, G. D.; Buehler, E.; Storz, F. G. *Appl. Phys. Lett.* **1971**, *18*, 301.

(9) Ohmer, M. C.; Pandey, R. *MRS Bull.* **1998**, *23*, 16.

(10) (a) Isaenko, L.; Vasilyeva, I.; Merkulov, A.; Yelisseyev, A.; Lobanov, S. *J. Cryst. Growth* **2005**, *275*, 217. (b) Isaenko, L.; Yelisseyev, A.; Lobanov, S.; Krinitsin, P.; Petrov, V.; Zondy, J. J. *J. Non-Cryst. Solids* **2006**, *352*, 2439.

(11) Lin, X. S.; Zhang, G.; Ye, N. *Cryst. Growth Des.* **2009**, *9*, 1186.

(12) Yao, J. Y.; Mei, D. J.; Bai, L.; Lin, Z. S.; Yin, W. L.; Fu, P. Z.; Wu, Y. C. *Inorg. Chem.* **2010**, *49*, 9212.

(13) (a) Petrov, V.; Badikov, V.; Shevyrdyaeva, G.; Panyutin, V.; Chizhikov, V. *Opt. Mater.* **2004**, *26*, 217. (b) Schunemann, P. G.; Zawilski, K. T.; Pollak, T. M. J. *Cryst. Growth* **2006**, *287*, 248.
(14) Kim, Y.; Seo, I. S.; Martin, S. W.; Baek, J.; Halasyamani, P. S.; Arumugam, N.; Steinfink, H. *Chem. Mater.* **2008**, *20*, 6048.
(15) Mei, D. J.; Yin, W. L.; Feng, K.; Lin, Z. S.; Bai, L.; Yao, J. Y.; Wu, Y. C. *Inorg. Chem.* **2011**, *51*, 1035−1040.
(16) (a) Lin, X. S.; Guo, Y. F.; Ye, N. *J. Solid State Chem.* **2012**, *195*, 172. (b) Yin, W. L.; Feng, K.; He, R.; Mei, D. J.; Lin, Z. S; Yao, J. Y.; Wu, Y. C. *Dalton Trans.* **2012**, *41*, 5653.
(17) Chen, M. C.; Li, P.; Zhou, L. J.; Li, L. H.; Chen, L. *Inorg. Chem.* **2011**, *50*, 12402.
(18) Eulenberger, G. *Z. Naturforsch. B* **1980**, *35*, 335.
(19) Marking, G. A.; Kanatzidis, M. G. *J. Alloys Compd.* **1997**, *259*, 122.
(20) Palchik, O.; Marking, G. M.; Kanatzidis, M. G.. *Inorg. Chem.* **2005**, *44*, 4151.
(21) Aitken, J. A.; Larson, P.; MahantiS, D.; Kanatzidis, M. G. *Chem. Mater.* **2001**, *13*, 4714.
(22) Aitken, J. A.; Marking, G. A.; Evain, M.; Iordanidis, L.; Kanatzidis, M. G. *J. Solid State Chem.* **2000**, *153*, 158.
(23) Mazurier, A.; Jaulmes, S.; Guittard, M. *Acta Crystallogr., Sect. B: Struct. Crystallogr. Cryst. Chem.* **1980**, *36*, 1990.
(24) Riga, M. Y. *Inorg. Mater.* **2005**, *41*, 65.
(25) Huang, Y. Z.; Wu, L. M.; Wu, X. T.; Li, L. H.; Chen, L.; Zhang, Y. F. *J. Am. Chem. Soc.* **2010**, *132*, 12788.
(26) Yin, W. L.; Feng, K.; Mei, D. J.; Yao, J. Y.; Fu, P. Z.; Wu, Y. C. *Dalton Trans.* **2012**, *41*, 2272.
(27) *CrystalClear*, Version 1.3.5; Rigaku Corp.: The Woodlands, TX, 1999.
(28) Sheldrick, G. M. *SHELXTL*, Version 5.1; Bruker-AXS: Madison, WI, 1998.
(29) Spek, A. L. *J. Appl. Crystallogr.* **2003**, *36*, 7.
(30) (a) Brown, I. D.; Altermatt, D. *Acta Crystallogr., Sect. B: Struct. Sci.* **1985**, *41*, 244. (b) Brese, N. E.; Okeeffe, M. *Acta Crystallogr., Sect. B: Struct. Sci.* **1991**, *47*, 192.
(31) Kortüm, G. *Reflectance Spectroscopy*; Springer−Verlag: New York, 1969.
(32) Kurtz, S. K.; Perry, T. T. *J. Appl. Phys.* **1968**, *39*, 3798.
(33) Kresse, G.; Furthmüller, J. *Phys. Rev. B* **1996**, *54*, 11169.
(34) Perdew, J. P.; Wang, Y. *Phys. Rev. B* **1992**, *45*, 13244.
(35) (a) Kresse, G.; Joubert, D. *Phys. Rev. B* **1999**, *59*, 1758. (b) BlÖchl, P. E. *Phys. Rev. B* **1994**, *50*, 17953.
(36) Blöchl, P. E.; Jepsen, O.; Andersen, O. K. *Phys. Rev. B* **1994**, *49*, 16223.
(37) Ching, W. Y. *J. Am. Ceram. Soc.* **1990**, *73*, 3135.
(38) Laksari, S.; Chahed, A.; Abbouni, N.; Benhelal, O.; Abbar, B. *Comput. Mater. Sci.* **2006**, *38*, 223.
(39) Mo, S. D.; Ching, W. *Phys. Rev. B* **1995**, *51*, 13023.
(40) Aversa, C.; Sipe, J. E. *Phys. Rev. B* **1995**, *52*, 14636.
(41) Rashkeev, S. N.; Lambrecht, W. R. L.; Segall, B. *Phys. Rev. B* **1998**, *57*, 3905.
(42) Egorova, B. V.; Olenev, A. V.; Berdonosov, P. S.; Kuznetsov, A. N.; Stefanovich, S. Y.; Dolgikh, V. A.; Mahenthirarajah, T.; Lightfoot, P. *J. Solid State Chem.* **2008**, *181*, 1891.
(43) (a) Ravindran, P.; Delin, A.; Ahuja, R.; Johansson, B.; Auluck, S.; Wills, J. M.; Eriksson, O. *Phys. Rev. B* **1997**, *56*, 6851. (b) Haiying, He.; Orlando, R.; Blanco, M. A.; Pandey, R.; Amzallag, E.; Baraille, I.; Rerat, M. *Phys. Rev. B* **2006**, *74*, 195123.